



2017

Slowly cycling Rho kinase-dependent actomyosin cross-bridge "slippage" explains intrinsic high compliance of detrusor smooth muscle

Christopher J. Neal
Virginia Commonwealth University

Jia B. Lin
Virginia Commonwealth University

Tanner Hurley
Virginia Commonwealth University

See next page for additional authors

Follow this and additional works at: http://scholarscompass.vcu.edu/bioc_pubs

 Part of the [Medicine and Health Sciences Commons](#)

Copyright © 2017 the American Physiological Society

Downloaded from

http://scholarscompass.vcu.edu/bioc_pubs/41

This Article is brought to you for free and open access by the Dept. of Biochemistry and Molecular Biology at VCU Scholars Compass. It has been accepted for inclusion in Biochemistry and Molecular Biology Publications by an authorized administrator of VCU Scholars Compass. For more information, please contact libcompass@vcu.edu.

Authors

Christopher J. Neal, Jia B. Lin, Tanner Hurley, Amy S. Miner, John E. Speich, Adam P. Klausner, and Paul H. Ratz

RESEARCH ARTICLE

Slowly cycling Rho kinase-dependent actomyosin cross-bridge “slippage” explains intrinsic high compliance of detrusor smooth muscle

Christopher J. Neal,² Jia B. Lin,¹ Tanner Hurley,¹ Amy S. Miner,¹ John E. Speich,² Adam P. Klausner,³ and Paul H. Ratz¹

¹Department of Biochemistry and Molecular Biology, Virginia Commonwealth University, Richmond, Virginia; ²Department of Mechanical and Nuclear Engineering, Virginia Commonwealth University, Richmond, Virginia; and ³Department of Surgery, Virginia Commonwealth University, Richmond, Virginia

Submitted 30 November 2016; accepted in final form 22 March 2017

Neal CJ, Lin JB, Hurley T, Miner AS, Speich JE, Klausner AP, Ratz PH. Slowly cycling Rho kinase-dependent actomyosin cross-bridge “slippage” explains intrinsic high compliance of detrusor smooth muscle. *Am J Physiol Renal Physiol* 313: F126–F134, 2017. First published March 29, 2017; doi:10.1152/ajprenal.00633.2016.—Biological soft tissues are viscoelastic because they display time-independent pseudoelasticity and time-dependent viscosity. However, there is evidence that the bladder may also display plasticity, defined as an increase in strain that is unrecoverable unless work is done by the muscle. In the present study, an electronic lever was used to induce controlled changes in stress and strain to determine whether rabbit detrusor smooth muscle (rDSM) is best described as viscoelastic or viscoelastic plastic. Using sequential ramp loading and unloading cycles, stress-strain and stiffness-stress analyses revealed that rDSM displayed reversible viscoelasticity, and that the viscous component was responsible for establishing a high stiffness at low stresses that increased only modestly with increasing stress compared with the large increase produced when the viscosity was absent and only pseudoelasticity governed tissue behavior. The study also revealed that rDSM underwent softening correlating with plastic deformation and creep that was reversed slowly when tissues were incubated in a Ca²⁺-containing solution. Together, the data support a model of DSM as a viscoelastic-plastic material, with the plasticity resulting from motor protein activation. This model explains the mechanism of intrinsic bladder compliance as “slipping” cross bridges, predicts that wall tension is dependent not only on vesicle pressure and radius but also on actomyosin cross-bridge activity, and identifies a novel molecular target for compliance regulation, both physiologically and therapeutically.

bladder; biomechanics; contraction; blebbistatin; cytochalasin D; ROCK

SOFT TISSUES SUCH AS SKIN and muscle are classified as viscoelastic materials because they are reported to display time-independent elasticity (springlike behavior) and time-dependent viscosity (fluidlike resistance to deformation), and because they return to their original length after removal of a deforming force (13, 39). This classification permits biomechanical computer (in silico) modeling of complex tissues and organs, such as the urinary bladder (1, 14, 21, 24, 25, 34), in an attempt to better interpret information, make predictions, and simulate

conditions relevant to understanding material changes that take place under certain pathologies (15, 36). However, in silico models have not yet provided a comprehensive description of normal and pathological bladder behavior (23), indicating that additional studies are required to biomechanically characterize detrusor smooth muscle (DSM).

Urologists rely on pressure-volume (cystometric) analyses (29) to diagnose urological disorders. By exploiting certain transformations that relate wall stress to vesicle pressure, radius, and wall thickness (i.e., the Laplace relationship), the description of the bladder as a viscoelastic material permits calculations of wall tension, as well as extrapolation from one- and two-dimensional stress-strain material characteristics examined in vitro to three-dimensional whole organ pressure-volume behavior. Several assumptions are necessary to validate such transformations, including that the tissue is elastic, pseudoelastic or viscoelastic, and thus returns to its original length after removal of a deforming force. However, a few early studies provide evidence that the bladder does not return to its original length after removal of a deforming force, suggesting that, in addition to viscoelasticity, the bladder displays plastic behavior (1, 2). Notably, the bladder is known to be highly compliant during much of the filling phase (large increase in volume for a given increase in pressure) (40) compared with, for example, the systemic vasculature (37), suggesting that minimal force is developed when DSM is lengthened, but the precise biomechanics of DSM stress-strain behavior remain to be fully elucidated. Our laboratory and others have shown that bladder (33) and gastrointestinal smooth muscles (16, 22) can be strain softened. Furthermore, “slippage” of slowly cycling actomyosin cross bridges in tissues incubated in a Ca²⁺-free solution to abolish active contraction (19, 28, 35) appears to be responsible for the “resting” force softened by strain, suggesting that cross bridges may participate in DSM plasticity. The goal of the present study was to more fully characterize the viscoelastic properties of isolated rabbit DSM (rDSM), and to determine whether rDSM can be described solely as a viscoelastic material, or as a viscoelastic material that also contains a plastic element.

METHODS

Animals. All studies were approved by the Institutional Animal Care and Use Committee of Virginia Commonwealth University and conform to the Public Health Service Policy on Humane Care and Use of Laboratory Animals and the National Research Council *Guide for*

Address for reprint requests and other correspondence: P. H. Ratz, Dept. of Biochemistry and Molecular Biology, School of Medicine, Virginia Commonwealth University, PO Box 980614, 1101 East Marshall St., Richmond, VA 23298 (e-mail: paul.ratz@vcuhealth.org).

the Care and Use of Laboratory Animals. Specific pathogen-free, male, New Zealand White rabbits were obtained from Robinson Services (Mocksville, NC) and maintained in the vivarium at 19–22°C and a 12:12-h light-dark cycle for at least 6 to 7 days before experimentation. Animals were individually housed, provided environmental enrichment, and fed a combination of pelleted high-fiber rabbit food (Harlan Teklad 2031, ~1 cup/day) and hay.

Tissue preparation. Tissues were prepared as previously described (32). In short, urinary bladders were removed from euthanized rabbits and immediately placed in ice-cold physiological salt solution [PSS; composition in mM: 140 NaCl, 4.7 KCl, 1.2 Na₂HPO₄·7H₂O, 2.0 MOPS, 0.02 Na₂-ethylenediamine tetraacetic acid to chelate heavy metals, 5.6 D-glucose, 1.6 CaCl₂, and 1.2 MgCl₂, made with high-purity (17 MΩ) deionized water and adjusted using NaOH to a pH of 7.4]. A nominally Ca²⁺-free solution in which CaCl₂ was not added to the standard PSS also was used in this study. Thin strips of rDSM ~3 mm wide by ~100 μm thick were isolated from underlying mucosa by microdissecting longitudinal muscle bundles clearly visible under a stereo microscope (Olympus SZX12). Each muscle strip immersed in PSS in an aerated muscle bath heated to 37°C was secured by aluminum foil to the lever arm of a computer-driven dual-mode electronic lever (model 300B-LR, Aurora Scientific, Aurora, ON, Canada) to impose controlled length and force perturbations and measure resulting force and length changes, respectively (27), and a Delrin clip coupled to a micrometer (20-mm range, 10-μm graduations; 262M, L. S. Starrett, Athol, MA) for manual length adjustments. The initial slack length of each tissue between the clips was ~3 mm. Voltage signals to and from the lever were digitized using a multifunction data-acquisition board (PCI-6036E, National Instruments, Austin, TX) and stored on a computer at 1,000 Hz using a data-acquisition program (DASYLab 10, National Instruments).

Length-force analysis. Each rDSM strip was subjected to a full-length force analysis to identify a reference length (l_{ref}) that produced the maximum active force induced upon stimulation with 110 mM KCl (substituted isosmotically for NaCl). The force borne by the muscle at each length before stimulation with KCl was the preload force, also termed “resting” or “passive” force (26). After establishing l_{ref} , each tissue was positioned at 80% l_{ref} and contracted briefly (~30 s) two times using KCl as the stimulus to identify the degree of active contraction at 80% l_{ref} . The KCl was washed from the tissue each time with two changes of fresh PSS. Each KCl-induced contraction followed by washout-induced relaxation was termed a contraction-relaxation cycle. Tissues were considered ready for loading-unloading cycling once they had developed spontaneous low-amplitude rhythmic contractions. All subsequent studies on force and stress (force per tissue area), except where designated, examined the effects of tissue strain (normalized length) on preload force in tissues incubated in a nominally Ca²⁺-free PSS to ensure that spontaneous rhythmic (active) contractions were absent (33). Thus “force” and “stress” in all figures, except those panels identifying a KCl-induced contraction, refer to the preload force borne when tissues were not activated by a contractile stimulus. Force and stress were reported as millinewtons and kilopascals, respectively (26). Strain was calculated as the length, l , minus the initial length, l_0 , divided by the initial length [strain = $(l - l_0)/l_0$], or as the strain ratio (l/l_0) (13, 26). Stiffness in kilopascals was calculated as the incremental change in stress divided by the incremental change in strain and was plotted as a function of stress.

Protocols. Strips of rDSM were subjected to three sequential perturbations (protocols). A preconditioning protocol consisted of seven sequential ramp loading-unloading (L-UL) cycles (for example, Fig. 1A, A1–A7) (13). One or 10 min after preconditioning, the tissue was subjected to a single ramp L-UL cycle (for example, Fig. 1A, B1–1') to measure the degree of viscous return (Fig. 1B, B1–1'). Immediately following the viscous return protocol, each tissue was subjected to a preload force-recovery protocol consisting of incubation for 15 min in PSS, a contraction-relaxation cycle using KCl as the

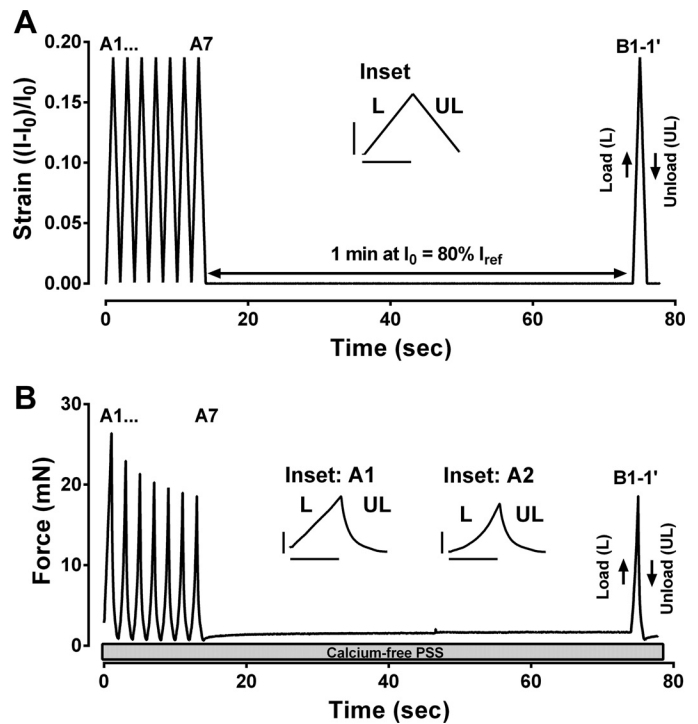


Fig. 1. Example of data from a preconditioning (A1 . . . A7) and viscous-return (B1-1') loading (L) and unloading (UL) protocol. A: strain. B: force. The horizontal bars in the insets equal 1 s. The vertical bar in the inset of A is strain = 0.1, and the vertical bars in the insets of B are stress = 10 mN. Data collected using preconditioning and viscous-return protocols occurred while tissues were incubated in a nominally Ca²⁺-free solution.

stimulus, and a single ramp L-UL cycle (see Fig. 4A). In all three protocols, the lever was programmed to stretch the muscle (loading, L) at a constant rate of 18.75% l_{ref}/s from an initial muscle length (l_0) of 80% l_{ref} to a final length of 98.75% l_{ref} , then immediately release the muscle (unloading, UL) at the same rate from 98.75% l_{ref} back to 80% l_{ref} . Thus each L-UL cycle was imposed at an overall rate of 0.5 Hz. The temporal changes in preload force induced by the ramp changes in length imposed on the muscle were recorded, and the maximum and minimum stress values were calculated. From the time-dependent strain and stress data, full stress-strain curves were calculated and plotted for both loading (see Figs. 2 and 4) and unloading (see Fig. 7).

Data analysis and statistics. All data were analyzed using Graph Pad Prism 6.0 software (GraphPad Software, La Jolla, CA) and are presented as representative tracings and as means \pm SE. The “ n ” value was the number of bladders, not the number of muscle strips. When two groups were compared for statistical analyses, data were evaluated by Student’s t -test, and the null hypothesis was normally rejected at $P < 0.05$. When group was compared more than once, Student’s t -test with the Bonferroni method was used. In the latter case, if one group was compared twice or three times, then the null hypothesis was rejected at, respectively, $P < 0.025$ or $P < 0.0125$.

RESULTS

Stress-strain curves produced by the preconditioning protocol. Over the course of seven sequential ramp L-UL cycles, each at 0.5 Hz (Fig. 1A, A1 . . . A7 and see inset for a zoomed image of a single cycle), the stress achieved at the end of each loading (i.e., the peak stress values, Fig. 1B) declined (softened) exponentially with a half-time ($t_{1/2}$) of 2.7 s ($r^2 = 0.99$). We designated the seventh cycle as representing a pseudo-steady-state set of values because, based on the $t_{1/2}$, the

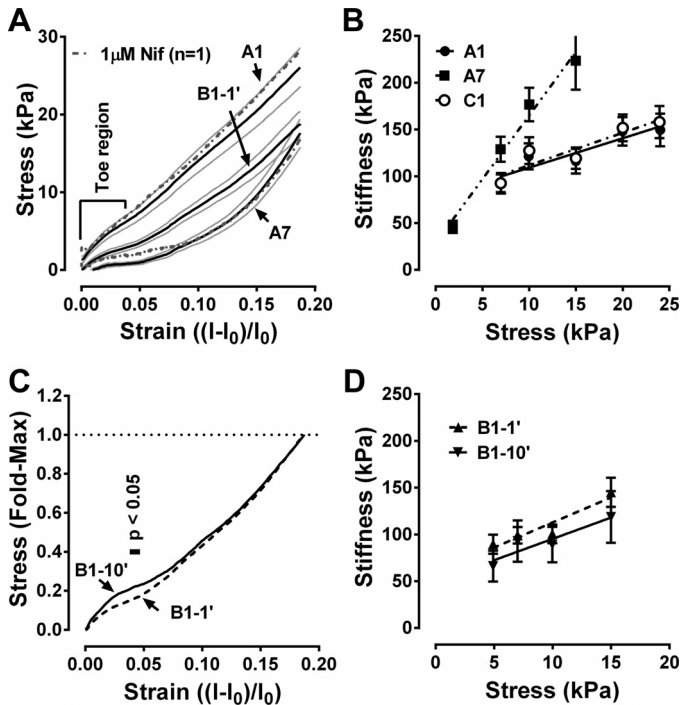


Fig. 2. Stress-strain (A and C) and stiffness-stress (B and D) analyses for the initial loading (A1; A and B) and final loading (A7; A and B) of the preconditioning protocol, and the single loading of the viscous-return protocol after wait periods of 1 min (B1-1'; A, C, and D) and 10 min (B1-10'; C and D). B: also shown for comparison is the stiffness-stress curve calculated for the preload force-recovery protocol (C1). A: values are means (solid lines) \pm SE (shaded lines); $n = 4$. All B1-1' stress data are significantly different from respective A1 stress data ($P < 0.025$), and A7 and B1-1' stress data are significantly different from strain = 0 to strain = 0.174 ($P < 0.025$). A: calcium channel blockade (1 μ M nifedipine, dashed-dotted shaded line, $n = 1$) appeared to permit softening just as incubation in a Ca^{2+} -free solution did. C: values are mean values (horizontal bar identifies strain range where stress values are different; $P < 0.05$). B and D: values are means \pm SE; $n = 8-9$.

maximum stress observed during the seventh cycle had achieved $\sim 97\%$ of the theoretical final steady-state maximum value. The minimum stress achieved at the end of each unloading fell by nearly 80% from the first to second L-UL cycle (Fig. 1B) and declined only slightly thereafter. Thus both maximum and minimum stress values achieved during the seventh L-UL cycle (A7 maximum: 15.9 ± 1.7 ; A7 minimum: 0.0 ± 0.2 ; $n = 9$) were significantly less than the respective values achieved during the first L-UL cycle (A1 maximum: 25.3 ± 2.7 ; A1 minimum: 1.6 ± 0.3 ; $n = 9$, $P < 0.05$). For cycle 1, the loading stress-strain curve was nearly linear (Fig. 1B, inset: A1, L), and the unloading curve was nonlinear and considerably weaker than the loading curve at comparable strain values (Fig. 1B, inset: A1, UL). Subsequent loading curves were nonlinear and weaker than the A1 loading curve (Fig. 1B, inset: A2, L), indicating that the tissue had softened. The area of the seventh cycle was less than that of the first cycle, indicating that the preconditioned tissue displayed lower viscosity than the non-preconditioned tissue.

Comparison of the initial loading stress-strain curve (A1, L) to those produced after preconditioning (A7, L) and by the viscous-return protocol (B1, L). The toe region of the stress-strain curve of A1 (Fig. 2A, values between 0 and ~ 7 kPa)

Table 1. Y-intercept (E_0) and slope of linear stiffness-stress curves

	A1, L	A7, L	B1, L	C1, L	UL
E_0 , kPa	77.8 ± 12.6	28.9 ± 12.6	54.5 ± 11.0	77.3 ± 14.4	12.3 ± 0.5
Slope	3.1 ± 0.8	13.6 ± 1.3	5.0 ± 1.1	3.5 ± 0.9	33.4 ± 0.1
n	9	8	8	8	9
r^2	0.85	0.98	0.91	0.84	0.98

Values are means \pm SE; n , no. of bladders. L, loading; UL, unloading. A1, A7, and B1 are defined in the text and in Fig. 1 legend, C1 is defined in the text and in Fig. 4 legend.

displayed an increase then decrease (spike) in stiffness when plotted as a stiffness-stress curve (not shown). When the toe region was excluded, the shape of the first loading stress-strain curve was nearly linear (Fig. 2A, A1), which resulted in a low slope in the linear stiffness-stress plot (Fig. 2B, A1, and Table 1). Because stiffness-stress curves of biological tissues generally display increasing stiffness with increasing stress, Fung's group (13, 38) introduced the term E_0 , the Y-intercept of the

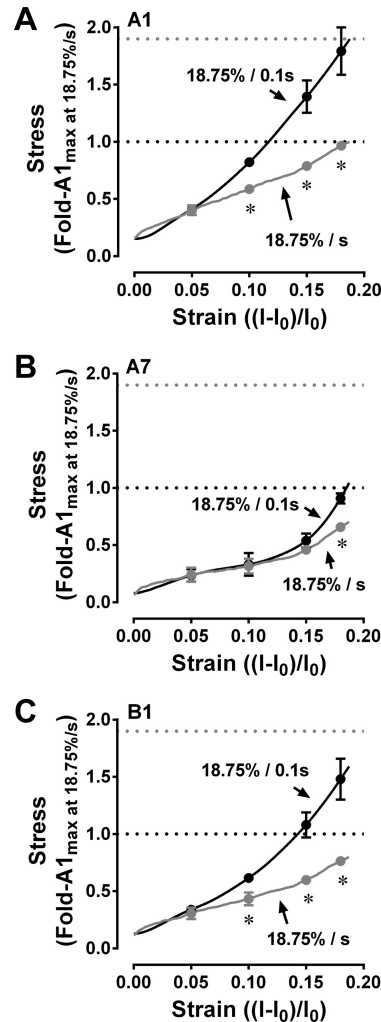


Fig. 3. Stress-strain curves resulting from ramp loading at the rate of strain used in all other studies (18.75%/s) and at a 10-fold higher rate (18.75%/0.1 s) for the first (A1; A) and last (A7; B) loading portions of the preconditioning protocol, and the loading portion of the viscous-return protocol (B1; C). Values are means \pm SE; $n = 3$. * $P < 0.05$, comparing slow to fast rates.

extrapolated linear stiffness-stress curve that, for the A1 curve, was relatively high (Table 1). The shape of the seventh loading curve was much more curvilinear than that of the first loading curve, resulting in a stiffness-stress plot (Fig. 2B, A7) displaying a higher slope and lower E_0 value (Table 1). That is, at stress values less than ~5 kPa, the preconditioned tissue represented by the A7 stress-strain curve was less stiff than that of the non-preconditioned tissue represented by the extrapolated A1 stress-strain curve, and, at stress values greater than ~5 kPa, the stiffness of the preconditioned tissue was increasingly much greater than that of the non-preconditioned tissue (Fig. 2B). A tissue incubated in a Ca^{2+} -containing solution (1.6 mM $CaCl_2$) in which 1 μ M nifedipine was included to block cellular Ca^{2+} entry produced responses similar to those produced by tissues incubated in a nominally Ca^{2+} -free solution (Fig. 2A, dashed-dotted shaded lines).

Although the maximum and minimum stress values induced by loading after a 1-min wait-period (viscous-return protocol, B1-1') were not elevated above those induced by the A7 loading, stress values between these extremes were increased (Fig. 2A, compare B1-1' to A7). Thus, the B1-1' stress-strain

curve had less curvature than the A7 stress-strain relationship, resulting in a stiffness-stress curve intermediate to A1 and A7 (compare Fig. 2D to Fig. 2B and see Table 1). There was a small but significant difference within a narrow range of the toe region when comparing the stress-strain curve produced after waiting 10 min (B1-10') to that produced after waiting 1 min (B1-1') before subjecting tissues to the viscous-return L-UL cycle (B1). This difference was evident when the curves were plotted as fold-maximum (Fig. 2C, region of significant difference is indicated by a short horizontal line below " $P < 0.05$ "). However, when excluding the toe region, the B1-1' and B1-10' stress-strain and stiffness-stress (Fig. 2D) curves were not different. The average stiffness-stress parameters calculated when combining data from B1-1' and B1-10' are presented in Table 1.

Together, these data support the hypothesis that rDSM behaved as a viscoelastic tissue during the first L-UL cycle, and that seven sequential ramp L-UL cycles caused preconditioning, such that rDSM behaved mechanically as a pseudoelastic rather than viscoelastic biomaterial (13) by the seventh cycle, as assessed by the A7 loading stress-strain and

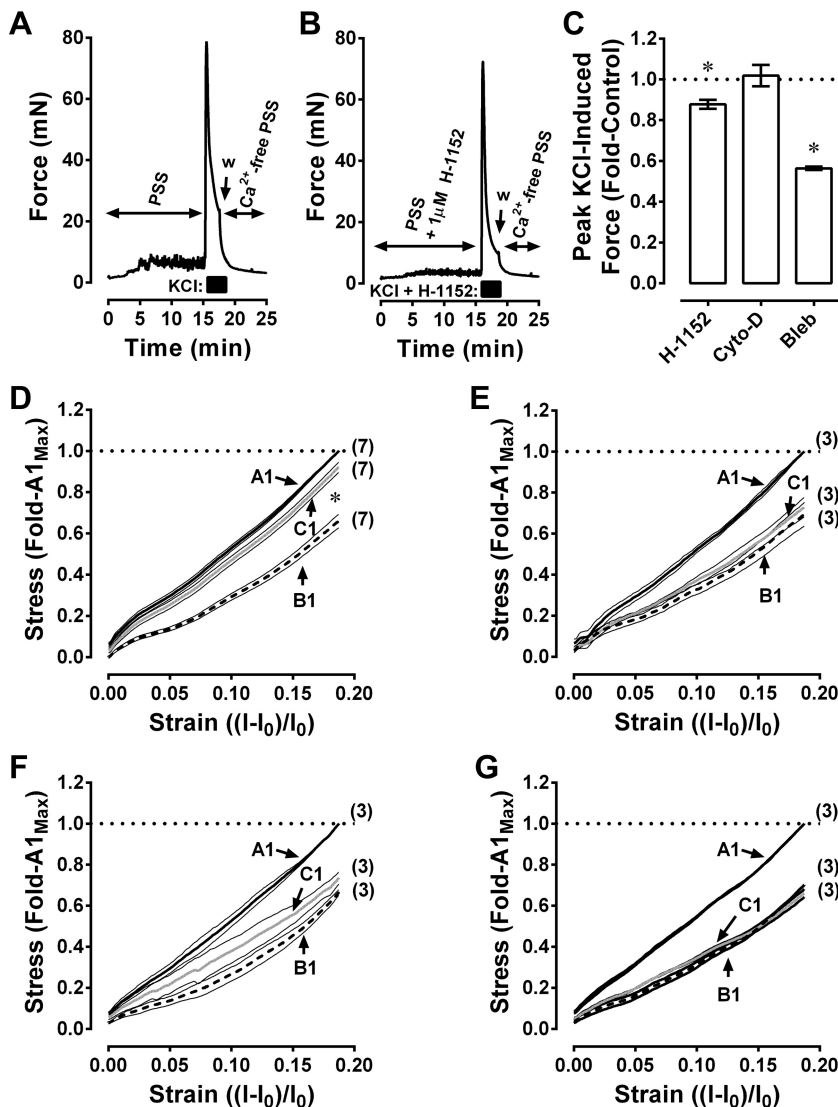


Fig. 4. Examples of contraction-relaxation cycles in the absence (A) and presence (B) of the Rho kinase inhibitor H-1152, and summary data showing the effects of inhibition of Rho kinase (H-1152; C), actin polymerization (Cyto-D; C), and actomyosin cross-bridge cycling (Bleb; C) on the peak force induced by KCl. Also shown are the loading stress-strain curves induced in a Ca^{2+} -free solution after the contraction-relaxation cycle (D-G) to assess whether inhibition of Rho kinase (E), actin polymerization (F), and actomyosin cross-bridge cycling (G) reduces the ability of the contraction-relaxation cycle to permit recovery of pre-load force compared with control tissues not exposed to a drug (D). Values in C are means \pm SE; $n = 3$. * $P < 0.05$ compared with 1.0. Values in D-G are means \pm SE (thin gray lines); n values are in parentheses. * $P < 0.05$ comparing C1 and B1.

stiffness-stress curves. This hypothesis was supported by an experiment revealing that the A1 (Fig. 3A) and B1 (Fig. 3C) loading stress-strain curves were highly sensitive to the rate of loading, as would be expected in a viscous material, and that, except at the longest strains, the A7 loading curve was insensitive to a 10-fold increase in the strain rate (Fig. 3B), as would be expected of a (pseudo)elastic material. The data presented in Fig. 2C support our model that rDSM viscosity may be represented by at least two viscous elements (34): one that returns relatively rapidly (within 1 min after completion of a 14-s preconditioning protocol), and one that returns more slowly and plays a mechanical role only at very low stress-strain values (within the toe region).

Comparison of the initial loading stress-strain curve (A1, L) to those produced by the viscous-return protocol (B1, L) and the preload force-recovery protocol (C1, L). At all strains examined, preload stress values induced during the B1–1' loading were significantly weaker than those induced during the A1 loading (Fig. 2A). We, therefore, tested the hypothesis that a contraction-relaxation cycle (Fig. 4A) would permit recovery (strengthening) of the softened preload force, as assessed by subsequently incubating the tissue in a nominally Ca²⁺-free solution and subjecting it to a single L-UL cycle that we termed “C1.” A single contraction-relaxation cycle permitted nearly full restoration of force, as assessed by the loading stress-strain curve (Fig. 4D, compare C1 to A1 and B1). Moreover, stiffness was fully restored, as revealed by the finding that stiffness-stress curve calculated for the C1 loading was superimposable on that calculated for the A1 loading (Fig. 2B, compare C1 to A1, and see Table 1).

To determine whether contractile proteins participated in the recovery of preload force, tissues were exposed to inhibitors of

Rho-associated protein kinase [1 μM H-1152 (Ref. 3), Fig. 4B], actomyosin cross bridges [30 μM blebbistatin (12)], and actin polymerization [0.2 μM cytochalasin D (4)] 15 min before and during the addition of KCl. Before subjecting tissues to a L-UL cycle (C1) to test for force recovery, drugs were washed from the tissues, and spontaneous rhythmic (active) contractions were prevented by two washes in a nominally Ca²⁺-free solution (see Fig. 4B). KCl-induced peak force was inhibited weakly by H-1152 (~10%, Fig. 4C). Incubation with cytochalasin D had no effect on KCl-induced peak force (Fig. 4C, Cyto-D), and incubation with blebbistatin caused an ~50% inhibition (Fig. 4C, Bleb). As assessed by the loading stress-strain curves, H-1152 (Fig. 4E), cytochalasin D (Fig. 4F), and blebbistatin (Fig. 4G) each prevented force recovery, despite exerting very different levels of inhibition of active force induced by KCl (Fig. 4C). These data suggest that the softening of preload force by preconditioning was due to yielding and slippage of a pool of actomyosin cross bridges not identical to those responsible for stimulus-induced active contraction.

Plastic deformation, creep, and Ca²⁺-dependent slow reversal of plastic deformation. To test the hypothesis that rDSM undergoes plastic deformation, tissues subjected to a single contraction-relaxation cycle and washed in a nominally Ca²⁺-free solution to ensure that they remained quiescent (i.e., free of spontaneous rhythmic contractions, Fig. 5A) were subjected to a load-clamp protocol. This protocol consisted of a step-increase in preload stress (step-load, Fig. 5A, L) from ~10% to ~25% of that developed by KCl, at which time stress was held constant (isotonic hold, or load clamp) for ~5 min, then stress was decreased (step unload) and clamped at the original or a weaker stress level (Fig. 5A; square-wave L, clamp, and UL,

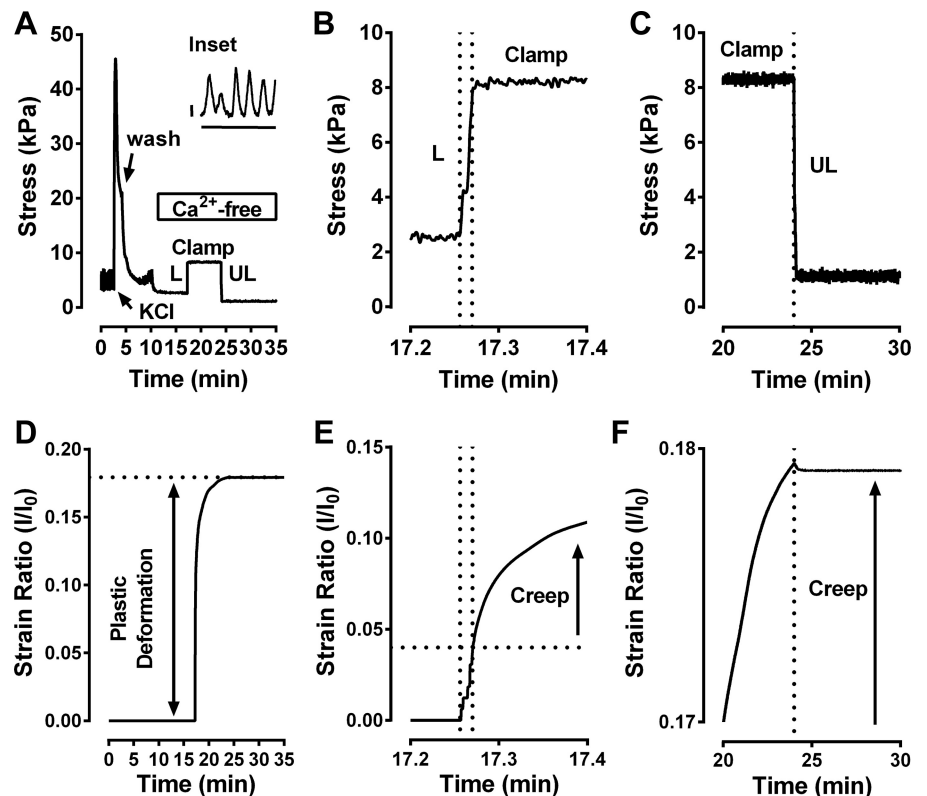


Fig. 5. Example of a contraction-relaxation cycle followed by a load-clamp protocol (A) and the resulting plastic deformation (D) that included the immediate strain (strain region between vertical dotted lines in E, which is a zoomed image of D) during loading (L, stress region between vertical dotted lines in B, which is a zoomed image of A), continued strain (Creep; E) during the load-clamp (Clamp; B) and absence of elastic recoil (F) upon unloading (UL; C). A: when incubated in a Ca²⁺-containing solution, the tissue usually developed spontaneous rhythmic contraction (stress data shown before addition of KCl, which is also shown as a zoomed stress-tracing in the inset). A: exposure to a Ca²⁺-free solution abolished rhythmic contraction.

and zoomed images of L and clamp, Fig. 5B; and load-clamp followed by UL, Fig. 5C). The step load caused an immediate lengthening (increase in strain, Fig. 5D, and zoomed image, Fig. 5E). Notably, the tissue continued to lengthen even as stress was held constant (clamped) at the new, higher level ("Creep", zoomed images, Fig. 5, E and F). Tissue creep ceased abruptly (Fig. 5D and zoomed image, Fig. 5F) upon unloading (Fig. 5C, UL), but muscle length did not return to its original value (Fig. 5D and zoomed image, Fig. 5F). That is, the tissue remained at its deformed length, which supports the hypothesis that rDSM contains a plastic element. Plastic deformation was not permanent if, during the step-load, load-clamp, step-unload protocol, tissues were maintained in a Ca²⁺-containing solution (Fig. 6, B, D, F, and H) instead of in a nominally Ca²⁺-free solution (Fig. 6, A, C, E, and G). Shortening of the tissue incubated in the Ca²⁺-containing

solution consisted of two components: a slow component corresponding with the step unload, and a very slow component corresponding with the load clamp at the original preload stress value (Fig. 6, F and H, zoomed images).

On average, tissues incubated in a Ca²⁺-free solution (n = 4) displayed plastic deformation with no recovery shortening upon unloading (Fig. 6I, Ca²⁺-free), whereas tissues incubated in a Ca²⁺-containing solution (n = 3) recovered ~55% of the plastic deformation within ~6 min (Fig. 6I, +Ca²⁺) by a combination of slow (0.00067 muscle lengths/s) and very slow (0.000083 muscle lengths/s) shortening (Fig. 6J). These rates are over three orders of magnitude slower than the maximum rate of muscle shortening in rabbit bladder (0.61 muscle lengths/s) (17).

For comparison, a rabbit renal artery incubated in a Ca²⁺-free solution was subjected to a load-clamp protocol (Fig. 6K;

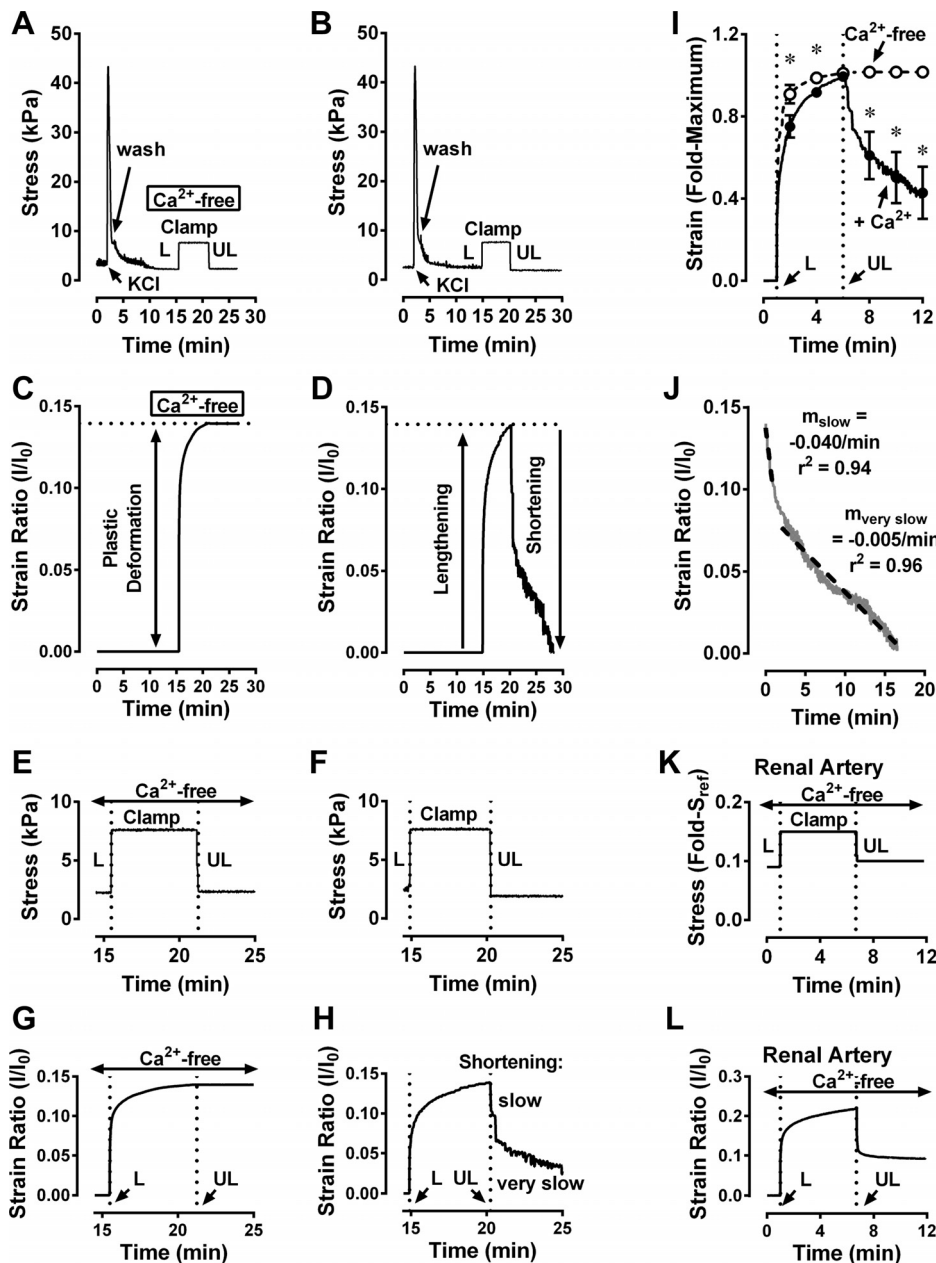


Fig. 6. Examples of a Ca²⁺-free, load-clamp protocol (A) as in Fig. 5, a modified load-clamp protocol in which tissues remained in a Ca²⁺-containing solution (B), and the resulting permanent plastic deformation that occurred when tissues were in a Ca²⁺-free solution (C) compared with slow and very slow recovery of plastic deformation that occurred when tissues were in a Ca²⁺-containing solution (D). E and F: zoomed images of A and B, respectively. G and H: zoomed images of C and D, respectively. I: average data comparing strain values resulting from Ca²⁺-free and Ca²⁺-containing load-clamp protocols; n = 3. *P < 0.05. J: average data fit by linear regression analysis revealing slow and very slow spontaneous muscle shortening. Also shown is an example of the strain changes (L) produced by a rabbit renal artery subjected to a Ca²⁺-free load-clamp protocol (K).

step increase in preload was from ~9 to ~15% of a KCl peak contraction, S_{ref}). Strain in renal artery (Fig. 6L), like that in rDSM (Fig. 6G), increased immediately upon the step load, then underwent creep (Fig. 6L) during the load clamp at the higher stress (Fig. 6K). Unlike rDSM (Fig. 6G, UL), rabbit renal artery did not remain at the longer strain (Fig. 6L, UL) when the tissue was unloaded, but immediately “snapped back,” although only by ~50% (Fig. 6K, UL). Together, these data suggest that plastic deformation may be a feature common to different smooth muscle types, and that the degree of plastic deformation in rDSM is greater than that in arterial smooth muscle. Moreover, the data suggest that Ca^{2+} -dependent slowly cycling cross-bridge activity is responsible for adjusting the degree of plastic deformation.

Stress-strain analysis during unloading. The stress-strain relationships calculated from the unloading portion of the first (Fig. 7A, A1) and seventh (Fig. 7B, A7) sequential L-UL cycles, from the viscous-return L-UL cycle (Fig. 7C, B1), and from the force-recovery L-UL cycle (Fig. 7D, C1) fit a curve

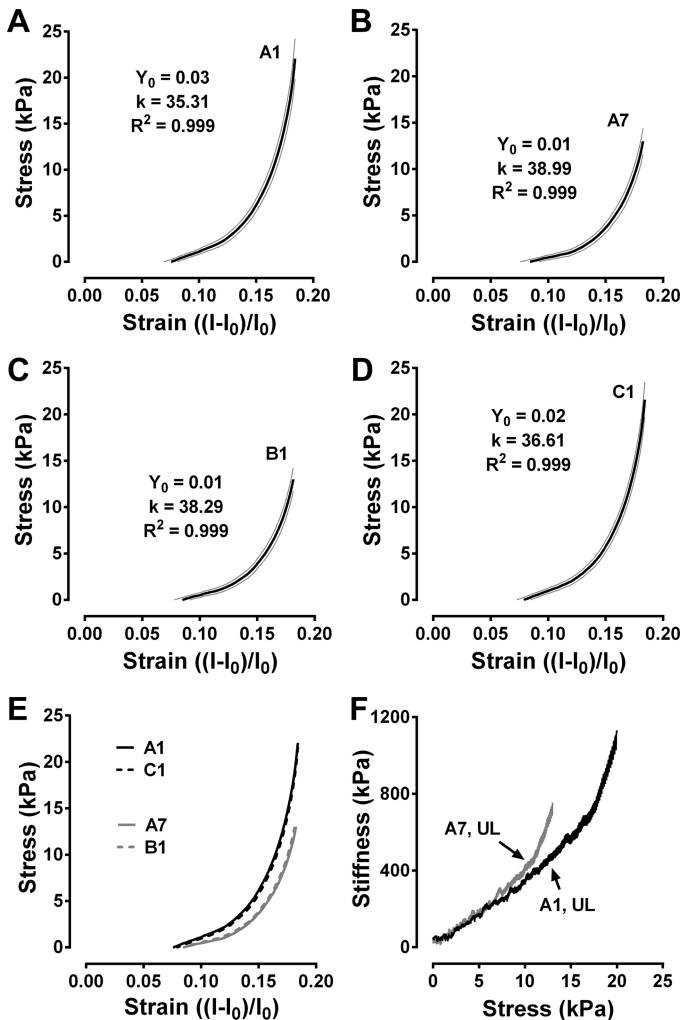


Fig. 7. Unloading stress-strain curves of the first (A1; A) and last (A7; B) loading-unloading cycles of the preconditioning protocol, the viscous-return protocol (B1; C), and the preload force-recovery protocol (C1; D). Values in A–D are means (solid lines) \pm SE (shaded lines); $n = 8$ –9. E: average data plotted together. F: average stiffness-stress curves for unloading (UL) during cycles A1 and A7.

described by a single exponential (stress = $Y_0 e^{k \times \text{strain}}$), with $Y_0 \sim 0$ and k ranging from ~35 to ~39. A7 and C1 UL curves were superimposable, as were A7 and B1 UL curves (Fig. 7E). Stiffness-stress curves were superimposable at low-strain values (Fig. 7F), and the linear portion of the curve displayed a lower E_0 value and higher slope compared with loading curves (Table 1).

DISCUSSION

The present study identifies rDSM as a viscoelastic plastic material. Thus the proposal that all soft biological tissues are viscoelastic (13) can be expanded to include our finding that certain tissues, such as rDSM, can also undergo plastic deformation. Notably, unlike nonbiological materials, where plastic deformation is irreversible, plastic deformation of live rDSM is reversible. Based on our data, we propose a working hypothesis that spontaneously active, slowly cycling, actomyosin cross bridges in rDSM represent a reversible frictional element that alternately “slips” to lengthen and contracts to shorten when an opposing force is, respectively, stronger and weaker than the force borne by the cross bridges. In vitro, when the tissue was incubated in a nominally Ca^{2+} -free solution to abolish cross-bridge cycling, the frictional element slipped (deformed) upon loading the tissue, and, upon unloading, the deformation remained, revealing the intrinsic plasticity. We found that the frictional element also slipped when loading while the tissues were incubated in a Ca^{2+} -containing solution. However, upon unloading, rDSM shortened in a biphasic pattern, resulting in an initial slow, then very slow, reversal of plastic deformation. We propose that, in vivo, ongoing adjustments of the linear position of the rDSM actomyosin motors endow the bladder with a mechanism to maintain a relatively constant wall tension over a broad range of vesicular volumes during filling. That is, we propose that the Laplace relationship cannot accurately describe bladder biomechanics because the bladder’s wall is not purely viscoelastic, but, instead, is a viscoelastic, reversibly plastic material.

We have shown that rabbit, mouse, and human bladders display reversible strain softening (6, 7, 28, 33, 36). These results, in conjunction with the present data, suggest that bladder compliance is a regulated parameter, and that compliance regulation is dependent on the regulation of actomyosin cross-bridge activity. If the bladder wall is modeled as a viscoelastic material, then, according to the Laplace relationship, vesicle radius, wall thickness, and pressure provide sufficient parameters to accurately calculate bladder wall tension, the major sensor of bladder fullness relayed to the central nervous system via afferent nerves (9, 18, 30, 41). Our data indicate that a fourth parameter, actomyosin cross-bridge activity, must also be included. Notably, our data indicate that the regulation of bladder actomyosin cross-bridge activity, and thus plasticity and compliance, represents a novel molecular focus for investigators interested in mechanisms causing, and therapies addressing, lower urinary tract disorders involving dysfunctional bladder contraction.

Currently, no models explain how the urinary bladder remains highly compliant upon filling. There is evidence suggesting that the urinary bladder is never quiescent, even during the filling phase (8, 10, 11). In particular, during bladder filling, cross-bridge activity of DSM appears to sequentially (rhyth-

mically “turn on” (contract) and “turn off” (relax) because DSM undergoes slow, low-amplitude, rhythmic contractions (5, 20, 31). We propose a model that incorporates rhythmic contractions during filling with plastic deformation that potentially explains high compliance during bladder filling. During bladder filling, DSM cells that are on the falling phase of the rhythmic contraction (relaxed) can undergo cross-bridge slippage and plastic deformation, permitting accommodation of an increased volume. Partial recovery of the plastic deformation can occur when DSM cells are contracting (on the rising phase of the rhythmic contraction). This model is consistent with our clinical study revealing the dynamic nature of compliance involving load-induced increases in compliance during filling that are reversed by a voiding contraction (6).

Fung (13) revealed that, although the loading and unloading curves of biological tissues after preconditioning display some hysteresis, the curves are highly stable (there is no further weakening with continued cycling), and the hysteresis loop is relatively independent of strain rate, a characteristic of elasticity. Thus Fung used the term pseudoelastic to distinguish this behavior from an ideal elastic material in which loading and unloading curves are nearly superimposable (display little hysteresis), and he considered the loading and unloading curves as representing two distinct elastic materials. rDSM displayed the least amount of hysteresis after preconditioning. Moreover, the loading curve after preconditioning was stable and insensitive to a 10-fold increase in strain rate, suggesting that the preconditioned rDSM could be modeled as two distinct pseudoelastic materials.

Elastic arteries utilize extracellular matrix proteins that are not acutely regulated when opposing the stresses induced by ventricular ejection of blood. In the dog thoracic aorta, the E_0 value extrapolated from the linear region of the pseudoelastic stress-strain curve is high (~90 kPa), and the slope is low (~1–1.5) (13, 38). Interestingly, the E_0 value and slope of the stiffness-stress curve of rDSM before preconditioning that reflect viscosity and cross bridges (see Fig. 2B, A1 and C1) were more similar to those identified for dog elastic artery than the values of rDSM after preconditioning that reflects elasticity (see Fig. 2B, A7). Thus, unlike aorta, rDSM when exposed to Ca^{2+} -free or Ca^{2+} -containing solutions appears to utilize adjustable actomyosin cross bridges and viscosity at low-stress values to oppose expanding stresses. When slowly cycling, cross bridges would be expected to slip upon loading, permitting accommodation. During the loading induced by a further increase in vesicular volume, rDSM elasticity, which has a higher stiffness-stress slope and lower E_0 value, would become engaged due to load transfer to resist further expansion. In summary, these data support the hypothesis that DSM viscosity and actomyosin cross bridges act to resist muscle lengthening at low stresses and short strains, and DSM elasticity acts at higher stress and longer strains, possibly preventing extreme distortion due to intermittent external mechanical insults (e.g., body movements). Alterations in actomyosin cross-bridge regulation may be expected to affect bladder compliance and the sensation of urgency. Our model proposing that bladder compliance is acutely adjusted during filling identifies actomyosin cross-bridge regulation as a novel target for potential therapeutic intervention of bladder dysfunction involving bladder over- and underactivity.

Study limitations. Our study did not determine whether nonmuscle myosins contributed along with smooth muscle myosins to compliance regulation. Moreover, our study cannot rule out the possibility that other proteins acted in concert with cross bridges. In particular, our study used a nominally Ca^{2+} -free solution to abolish Ca^{2+} -dependent rhythmicity and permit compliance analyses without the interference of spontaneously active contractions. Certain extracellular proteins involved in intercellular coupling, such as cadherins, also are Ca^{2+} sensitive and may have been affected by our nominally Ca^{2+} -free solution. To address this issue, we provided data in which tissues incubated in a Ca^{2+} -containing solution were treated with the Ca^{2+} channel blocker nifedipine to lower intracellular Ca^{2+} . The strain softening induced by a load-unload cycle in this tissue was similar to that induced in tissues exposed to a Ca^{2+} -free solution (see Fig. 2A, dashed-dotted lines compared with solid lines), suggesting that extracellular Ca^{2+} -dependent proteins did not play a role. However, this is a preliminary finding ($n = 1$), and a more definitive conclusion on this issue will require a more extensive analysis.

Potential clinical relevance. The urinary bladder is highly compliant, permitting accommodation of high urine volumes at low vesicular pressures. The present study identifies the molecular mechanism of bladder compliance as actomyosin cross-bridge slippage. Because cross bridges are regulated during bladder filling, these data indicate that the state of detrusor smooth muscle activation determines the degree of bladder compliance.

GRANTS

This work was supported, in part, by a Virginia Commonwealth University Department of Surgery Research Grant.

DISCLOSURES

No conflicts of interest, financial or otherwise, are declared by the author(s).

AUTHOR CONTRIBUTIONS

C.J.N., J.B.L., T.H., and A.S.M. performed experiments; C.J.N., J.B.L., and P.H.R. analyzed data; C.J.N. and P.H.R. interpreted results of experiments; J.E.S., A.P.K., and P.H.R. edited and revised manuscript; P.H.R. conceived and designed research; P.H.R. prepared figures; P.H.R. drafted manuscript; P.H.R. approved final version of manuscript.

REFERENCES

1. Alexander RS. Mechanical properties of urinary bladder. *Am J Physiol* 220: 1413–1421, 1971.
2. Alexander RS. Viscoplasticity of smooth muscle of urinary bladder. *Am J Physiol* 224: 618–622, 1973.
3. Alvarez SM, Miner AS, Browne BM, Ratz PH. Failure of Bay K 8644 to induce RhoA kinase-dependent calcium sensitization in rabbit blood vessels. *Br J Pharmacol* 160: 1326–1337, 2010. doi:10.1111/j.1476-5381.2010.00751.x.
4. Bednarek ML, Speich JE, Miner AS, Ratz PH. Active tension adaptation at a shortened arterial muscle length: inhibition by cytochalasin-D. *Am J Physiol Heart Circ Physiol* 300: H1166–H1173, 2011. doi:10.1152/ajpheart.00009.2010.
5. Byrne MD, Klausner AP, Speich JE, Southern JB, Habibi JR, Ratz PH. Fourier transform analysis of rabbit detrusor autonomous contractions reveals length dependent increases in tone and slow wave development at long lengths. *J Urol* 190: 334–340, 2013. doi:10.1016/j.juro.2013.02.071.
6. Colhoun AF, Klausner AP, Nagle AS, Carroll AW, Barbee RW, Ratz PH, Speich JE. A pilot study to measure dynamic elasticity of the bladder during urodynamics. *Neurourol Urodyn* 36: 1086–1090, 2017. doi:10.1002/nau.23043.
7. Colhoun AF, Speich JE, Dolat MT, Habibi JR, Guruli G, Ratz PH, Barbee RW, Klausner AP. Acute length adaptation and adjustable

- preload in the human detrusor. *NeuroUrol Urodyn* 35: 792–797, 2016. doi:10.1002/nau.22820.
8. Coolsaet BLRA, Blaivas JG. No detrusor is stable. *NeuroUrol Urodyn* 4: 259–261, 1985. doi:10.1002/nau.1930040402.
 9. Downie JW, Armour JA. Mechanoreceptor afferent activity compared with receptor field dimensions and pressure changes in feline urinary bladder. *Can J Physiol Pharmacol* 70: 1457–1467, 1992. doi:10.1139/y92-206.
 10. Drake MJ, Harvey IJ, Gillespie JI. Autonomous activity in the isolated guinea pig bladder. *Exp Physiol* 88: 19–30, 2003. doi:10.1113/eph8802473.
 11. Drake MJ, Harvey IJ, Gillespie JI, Van Duyl WA. Localized contractions in the normal human bladder and in urinary urgency. *BJU Int* 95: 1002–1005, 2005. doi:10.1111/j.1464-410X.2005.05455.x.
 12. Eddinger TJ, Meer DP, Miner AS, Meehl J, Rovner AS, Ratz PH. Potent inhibition of arterial smooth muscle tonic contractions by the selective myosin II inhibitor, blebbistatin. *J Pharmacol Exp Ther* 320: 865–870, 2007. doi:10.1124/jpet.106.109363.
 13. Fung YC. *Biomechanics*. New York: Springer-Verlag, 1993. doi:10.1007/978-1-4757-2257-4.
 14. Ghoniem GM, Regnier CH, Biancani P, Johnson L, Susset JG. Effect of vesical outlet obstruction on detrusor contractility and passive properties in rabbits. *J Urol* 135: 1284–1289, 1986.
 15. Gloeckner DC, Sacks MS, Fraser MO, Somogyi GT, de Groat WC, Chancellor MB. Passive biaxial mechanical properties of the rat bladder wall after spinal cord injury. *J Urol* 167: 2247–2252, 2002. doi:10.1016/S0022-5347(05)65137-3.
 16. Gregersen H, Emery JL, McCulloch AD. History-dependent mechanical behavior of guinea-pig small intestine. *Ann Biomed Eng* 26: 850–858, 1998. doi:10.1114/1.109.
 17. Hellstrand P, Johansson B. Analysis of the length response to a force step in smooth muscle from rabbit urinary bladder. *Acta Physiol Scand* 106: 221–238, 1979. doi:10.1111/j.1748-1716.1979.tb06392.x.
 18. Iggo A. Tension receptors in the stomach and the urinary bladder. *J Physiol* 128: 593–607, 1955. doi:10.1113/jphysiol.1955.sp005327.
 19. Jiang H, Liao D, Zhao J, Wang G, Gregersen H. Contractions reverse stress softening in rat esophagus. *Ann Biomed Eng* 42: 1717–1728, 2014. doi:10.1007/s10439-014-1015-7.
 20. Komari SO, Headley PC, Klausner AP, Ratz PH, Speich JE. Evidence for a common mechanism for spontaneous rhythmic contraction and myogenic contraction induced by quick stretch in detrusor smooth muscle. *Physiol Rep* 1: e00168, 2013. doi:10.1002/phy2.168.
 21. Korkmaz I, Rogg B. A simple fluid-mechanical model for the prediction of the stress-strain relation of the male urinary bladder. *J Biomech* 40: 663–668, 2007. doi:10.1016/j.jbiomech.2006.02.014.
 22. Liao D, Zhao J, Kunwald P, Gregersen H. Tissue softening of guinea pig oesophagus tested by the tri-axial test machine. *J Biomech* 42: 804–810, 2009. doi:10.1016/j.jbiomech.2009.01.029.
 23. Miftahof R, Nam HG. *Biomechanics of the Human Urinary Bladder*. Berlin: Springer, 2013. doi:10.1007/978-3-642-36146-3
 24. Nagatomi J, Gloeckner DC, Chancellor MB, DeGroat WC, Sacks MS. Changes in the biaxial viscoelastic response of the urinary bladder following spinal cord injury. *Ann Biomed Eng* 32: 1409–1419, 2004. doi:10.1114/B:ABME.0000042228.89106.48.
 25. Nagatomi J, Toosi KK, Chancellor MB, Sacks MS. Contribution of the extracellular matrix to the viscoelastic behavior of the urinary bladder wall. *Biomech Model Mechanobiol* 7: 395–404, 2008. doi:10.1007/s10237-007-0095-9.
 26. Ratz PH. Mechanics of Vascular Smooth Muscle. *Compr Physiol* 6: 111–168, 2015. doi:10.1002/cphy.c140072.
 27. Ratz PH, Murphy RA. Contributions of intracellular and extracellular Ca²⁺ pools to activation of myosin phosphorylation and stress in swine carotid media. *Circ Res* 60: 410–421, 1987. doi:10.1161/01.RES.60.3.410.
 28. Ratz PH, Speich JE. Evidence that actomyosin cross bridges contribute to “passive” tension in detrusor smooth muscle. *Am J Physiol Renal Physiol* 298: F1424–F1435, 2010. doi:10.1152/ajprenal.00635.2009.
 29. Rose DK. Cystometric bladder pressure determinations: Their clinical importance. *J Urol* 17: 487–501, 1927.
 30. Shea VK, Cai R, Crepps B, Mason JL, Perl ER. Sensory fibers of the pelvic nerve innervating the Rat’s urinary bladder. *J Neurophysiol* 84: 1924–1933, 2000.
 31. Shenfeld OZ, McCammon KA, Blackmore PF, Ratz PH. Rapid effects of estrogen and progesterone on tone and spontaneous rhythmic contractions of the rabbit bladder. *Urol Res* 27: 386–392, 1999. doi:10.1007/s002400050168.
 32. Shenfeld OZ, Morgan CW, Ratz PH. Bethanechol activates a post-receptor negative feedback mechanism in rabbit urinary bladder smooth muscle. *J Urol* 159: 252–257, 1998. doi:10.1016/S0022-5347(01)64077-1.
 33. Speich JE, Borgsmiller L, Call C, Mohr R, Ratz PH. ROK-induced cross-link formation stiffens passive muscle: reversible strain-induced stress softening in rabbit detrusor. *Am J Physiol Cell Physiol* 289: C12–C21, 2005. doi:10.1152/ajpcell.00418.2004.
 34. Speich JE, Quintero K, Dosier C, Borgsmiller L, Koo HP, Ratz PH. A mechanical model for adjustable passive stiffness in rabbit detrusor. *J Appl Physiol* (1985) 101: 1189–1198, 2006. doi:10.1152/japplphysiol.00396.2006.
 35. Speich JE, Southern JB, Henderson S, Wilson CW, Klausner AP, Ratz PH. Adjustable passive stiffness in mouse bladder: regulated by Rho kinase and elevated following partial bladder outlet obstruction. *Am J Physiol Renal Physiol* 302: F967–F976, 2012. doi:10.1152/ajprenal.00177.2011.
 36. Speich JE, Wilson CW, Almasri AM, Southern JB, Klausner AP, Ratz PH. Carbachol-induced volume adaptation in mouse bladder and length adaptation via rhythmic contraction in rabbit detrusor. *Ann Biomed Eng* 40: 2266–2276, 2012. doi:10.1007/s10439-012-0590-8.
 37. Stergiopoulos N, Meister JJ, Westerhof N. Evaluation of methods for estimation of total arterial compliance. *Am J Physiol Heart Circ Physiol* 268: H1540–H1548, 1995.
 38. Tanaka TT, Fung YC. Elastic and inelastic properties of the canine aorta and their variation along the aortic tree. *J Biomech* 7: 357–370, 1974. doi:10.1016/0021-9290(74)90031-1.
 39. Vincent JFV. *Structural Biomaterials*. Princeton, NJ: Princeton University Press, 2012.
 40. Wyndaele JJ, Gammie A, Bruschini H, De Wachter S, Fry CH, Jabr RI, Kirschner-Hermanns R, Madersbacher H. Bladder compliance what does it represent: can we measure it, and is it clinically relevant? *NeuroUrol Urodyn* 30: 714–722, 2011. doi:10.1002/nau.21129.
 41. Zagorodnyuk VP, Costa M, Brookes SJ. Major classes of sensory neurons to the urinary bladder. *Auton Neurosci* 126–127: 390–397, 2006. doi:10.1016/j.autneu.2006.02.007.